BIOCHEMISTRY

Article

Crystal Structures of Human and Murine Deoxyribonucleotidases: Insights into Recognition of Substrates and Nucleotide Analogues

Karin Walldn, Agnes Rinaldo-Matthis, Benedetta Ruzzenente, Chiara Rampazzo, Vera Bianchi, and Pr Nordlund

Biochemistry, **2007**, 46 (48), 13809-13818 • DOI: 10.1021/bi7014794

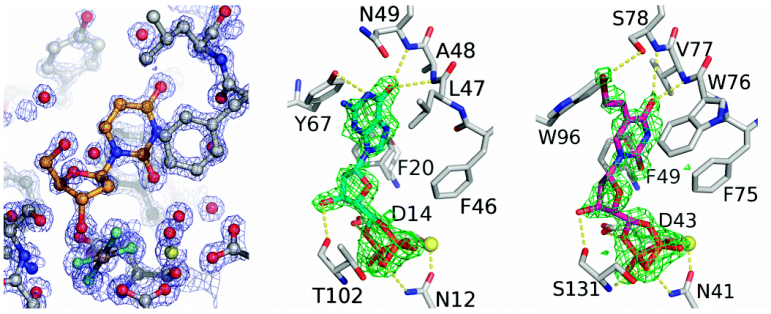

More About This Article

Additional resources and features associated with this article are available within the HTML version:

- Supporting Information
- Access to high resolution figures
- Links to articles and content related to this article
- Copyright permission to reproduce figures and/or text from this article

View the Full Text HTML

Crystal Structures of Human and Murine Deoxyribonucleotidases: Insights into Recognition of Substrates and Nucleotide Analogues†

Karin Walldén,‡,§ Agnes Rinaldo-Matthis,‡ Benedetta Ruzzenente,⊥ Chiara Rampazzo,⊥ Vera Bianchi,*,⊥ and Pär Nordlund*,§

Department of Biochemistry and Biophysics, Stockholm University, SE-106 91 Stockholm, Sweden, Department of Medical Biochemistry and Biophysics, Karolinska Institutet, SE-171 77 Stockholm, Sweden, and Department of Biology, University of Padova, I-35131 Padova, Italy

Received July 25, 2007; Revised Manuscript Received September 21, 2007

ABSTRACT: Cytosolic 5′(3′)-deoxyribonucleotidase (cdN) and mitochondrial 5′(3′)-deoxyribonucleotidase (mdN) catalyze the dephosphorylation of deoxyribonucleoside monophosphates and regulate dTTP formation in cytosol and mitochondria, protecting DNA replication from imbalanced precursor pools. They can also interfere with the phosphorylation-dependent activation of nucleoside analogues used in anticancer and antiviral treatment. To understand the relatively narrow substrate specificity of these two enzymes and their ability to use nucleotide analogues as substrates, we determined the crystal structures of human cdN in complex with deoxyuridine, murine cdN in complex with dUMP and dGMP, and human mdN in complex with the nucleotide analogues AZTMP and BVdUMP. Our results show that the active site residues Leu45 and Tyr65 in cdN form a more favorable binding surface for purine nucleotides than the corresponding Trp75 and Trp76 in mdN, explaining why cdN has higher activity for purine nucleotides than does mdN. The molecular interactions of mdN with AZTMP and BVdUMP indicate why these nucleotide analogues are poorer substrates as compared with the physiological substrate, and they provide a structural rationale for the design of drugs that are less prone to inactivation by the deoxyribonucleotidases. We suggest that introduction of substituents in the 3′-position may result in nucleoside analogues with increased resistance to dephosphorylation.

In mammals, ribo- and deoxyribonucleotides are synthesized either de novo from low-molecular-weight precursors or by salvage from nucleosides or nucleobases originating from catabolism of nucleic acids (*1*). In the salvage pathway, ribo- and deoxyribonucleosides are phosphorylated by nucleoside and nucleotide kinases to yield dNTPs and NTPs for DNA and RNA synthesis. The phosphorylation by cellular nucleoside kinases is opposed by 5′-nucleotidases that dephosphorylate ribo- and deoxyribonucleoside monophosphates (*2*, *3*).

Seven human 5′-nucleotidases are known, and they differ in substrate specificity, subcellular location, and tissue-specific expression (*2*, *3*). Cytosolic 5′(3′)-deoxyribonucleotidase (cdN)[1] and mitochondrial 5′(3′)-deoxyribonucleotidase (mdN) belong to this family of enzymes and share 52% sequence identity. They are specific for the deoxyribo form of nucleoside monophosphates, with dUMP and dTMP suggested as biological substrates. Unlike other family members they also dephosphorylate the 2′- or 3′-phosphates of pyrimidine ribonucleosides. The base specificity of mdN is unusually restricted for a 5′-nucleotidase, the enzyme being active almost exclusively with uracil- or thymine-containing nucleotides (*4*, *5*), whereas cdN works efficiently also with dGMP and dIMP (*6*, *7*).

Insight into the structural basis for substrate recognition in human 5′-nucleotidases is of biomedical importance since these enzymes may interfere with the phosphorylation-dependent activation of nucleoside analogues used in anticancer and antiviral treatment. Purified cdN and mdN dephosphorylate the monophosphate form of several nucleoside analogues (*5*). 5′-Nucleotidase activity has also been implicated in resistance to nucleoside analogues (*8*−*12*), and it was suggested that inhibitors of the enzymes might increase the efficacy of some analogues (*13*).

Of the mammal 5′-nucleotidases, structures have previously been solved of human mdN (*14*), human cytosolic 5′-nucleotidase II (cN-II) (*15*), human cytosolic 5′-nucleotidase III (cN-III) (pdb code 2CN1), and murine cN-III (*16*). Known intracellular 5′-nucleotidases belong to the structural haloacid

† This work was supported by grants from Telethon Italia (Grant GGP05001) (V.B.), AIRC Associazione Italiana per la Ricerca sul Cancro (V.B.), the Italian Ministry of Education and Research (Prin Project 2005) (V.B.), the University of Padova (C.R.), the Swedish Research Council (P.N.), the Swedish Cancer Society (P.N.), and from The European Community (Grant QLRT-CT-2000-01004).

* Correspondence may be addressed to either author. V.B.: tel., +39-049-8276282; fax, +39-049-8276280; e-mail, vbianchi@bio.unipd.it. P.N.: tel., +46-8-52486860; fax, +46-8-52486850; e-mail, Par.Nordlund@ki.se.

‡ Stockholm University.

§ Karolinska Institutet.

⊥ University of Padova.

[1] Abbreviations: cN-II, cytosolic 5′-nucleotidase II; cN-III, cytosolic 5′-nucleotidase III; cdN, cytosolic 5′(3′)-deoxyribonucleotidase; mdN, mitochondrial 5′(3′)-deoxyribonucleotidase; HAD, haloacid dehalogenase; AZT, 3′-azido-2′,3′-dideoxythymidine; BVdU, (*E*)-5-(2-bromovinyl)-2′-deoxyuridine. Monophosphates are abbreviated by addition of MP to the abbreviation of the nucleoside.

10.1021/bi7014794 CCC: $37.00
Published on Web 11/07/2007

dehalogenase (HAD) superfamily, which is defined by an α/β-Rossmann-like domain (core domain) and a smaller 4-helix bundle domain (cap domain). The cap domain is, however, not present in all HAD superfamily enzymes. Intracellular 5′-nucleotidases are dependent on Mg^{2+} for activity and share conserved residues in their active sites, suggesting that most of them have a similar catalytic mechanism. A conserved DXD motif is directly involved in the proposed mechanism for 5′-nucleotidases (*14*), in which the first Asp makes a nucleophilic attack on the phosphate of the nucleoside monophosphate and the second Asp donates a proton to the leaving nucleoside. The mechanism is believed to involve both a pentavalent substrate intermediate (*17*) and a phosphoenzyme intermediate (*18*, *19*). The cap domain is less structurally conserved than the core domain, binds the base of the nucleotide, and thereby determines the nucleobase specificity of 5′-nucleotidases (*14*, *15*, *20*).

We describe the crystal structures of human cdN in complex with deoxyuridine and murine cdN in complex with dUMP and dGMP. These constitute the first structures of cdNs and provide the structural background for the difference in substrate specificity between cdN and mdN. Furthermore, we present structures of mdN in complex with the nucleotide analogues AZTMP and BVdUMP. AZT is used in treatment of HIV (*21*, *22*), and BVdU is a potent inhibitor of herpes simplex virus type 1 and varicella-zoster virus (*23*). Together, the five structures show important sites of interaction between enzyme and substrate that we correlate with similarities and differences in specificity between cdN and mdN.

EXPERIMENTAL PROCEDURES

Preparation of Site-Specific Mutants. The inactive variants of human and murine cdN were obtained by introducing a mutated codon by PCR amplification of their cDNAs. The reaction required a single pair of primers because the amino acid to be substituted was close to the 5′-end of the coding sequence. For human cdN the primers used were ND10F (aat**catatg**gcgcggagctggcgcgtgctggtgAacatggac) and BD10R (aat**ggatcc**gcctgcccttccttttagctccagctgcctgccc), and for murine cdN the primers were D12NF (cata**catatg**gcggtgaagcggccgtgcgcgtgctggtgAacatggac) and D12NR (ctca**ggatcc**cctgtccacctcagggtccttcacaggctggctcgctt). Capital A's mark the nucleotide change introduced by the forward primers; bold letters indicate the 5′NdeI sites and the 3′BamHI sites introduced for subcloning. The D41N mutant of mdN was produced by site-directed mutagenesis as described previously (*20*).

The expression and purification of wild type and mutated human and murine cdN and of the D41N variant of mdN were performed as described previously (*4*, *7*), with the exception that the murine D12N mutant was produced in the *E. coli* Rosetta strain, designed for expression of proteins containing codons that are rare in bacteria. The two mutant cdN's had enzyme activities 6 orders of magnitude lower than the wild type recombinant enzymes, assayed as described (*7*).

Crystallization and Data Collection. All protein solutions used for crystallization contained 20 mM Tris buffer pH 7.5, 20% v/v glycerol, 2 mM DTT, 1 mM EDTA, and 75 mM NaCl. The protein concentration in the solution of human cdN was 9.0 mg/mL, of D12N 13.5 mg/mL, and of D41N 10.1 mg/mL. Protein concentrations were determined by the Bradford method (*24*) using bovine serum album as a standard. The hanging drop vapor diffusion method was used to grow crystals using drops with 1 μL of protein and 1 μL of reservoir solution. Human wild type cdN was crystallized in 50 mM KH_2PO_4, pH 4.5, and 2−15% (w/v) PEG8000 at 20 °C. D12N was crystallized in 0.2 M $MgCl_2$, 0.1 M Bis-Tris, pH 5.5, and 23−25% (w/v) PEG3350 at 6 °C. D41N was crystallized in 50 mM KH_2PO_4, pH 4.5, and 15−20% (w/v) PEG 8000 at 20 °C. The deoxyuridine complex was achieved by soaking the crystal in a reservoir solution with 10 mM deoxyuridine, 50 mM NaF, 5 mM $AlCl_3$, and 70 mM $MgCl_2$ for 60 min. The substrate and nucleoside analogue complexes were obtained by soaking the crystals for 45−60 min in reservoir solutions containing 10 mM substrate/nucleotide analogue. The nucleotide analogue soaks were also complemented with 90 mM $MgCl_2$. Data was collected on flash frozen crystals that had been soaked for 3−5 min (human cdN) or 10−20 s (murine cdN and mdN) in a cryo-solution containing 80% (v/v) reservoir solution and 20% (v/v) glycerol.

The D12N-dGMP and D41N-AZTMP data sets were collected at MaxLab II (Lund, Sweden) on beam-lines I711 and I911-5, respectively, the D12N-dUMP data set was collected on beam-line ID14.4 at the European Synchrotron Radiation Facility (Grenoble, France), and the cdN-deoxyuridine and D41N-BVdUMP data sets were collected on the beam-line X11 at the EMBL Hamburg Outstation (Germany). The cdN-deoxyuridine, D12N-dGMP, D41N-AZTMP, and D41N-BVdUMP data sets were processed with XDS and XSCALE (*25*), and the D12N-dUMP data set was processed with MOSFLM, version 6.2.5 (*26*), and SCALA (*27*).

Phasing, Model Building, and Refinement. The structure of human cdN was solved by molecular replacement using the CNS package (*28*) with an mdN structure (pdb code 1MH9) (*14*) as template resulting in a structure with two monomers in the asymmetric unit. The cross rotation search was made with a modeled dimer of mdN as a starting model. The first refinement cycle was made with CNS, and the remaining refinement cycles were made with REFMAC5.2 (*29*). Positive densities were seen after the first rigid body refinement corresponding to the ligands used in the soaking experiment. The Mg^{2+} ions were easily recognized due to the numbers of coordinating oxygen atoms and the distances to them (*30*). All residues, deoxyuridine, Mg^{2+}, and waters were built and refined initially with isotropic *B*-values. Then the *B*-values were refined anisotropically with a concomitant drop in *R*-values of about 4%. QUANTA (Accelrys, San Diego, CA) was used for model building.

The structure of murine cdN was solved by molecular replacement with MolRep (Version 9.2) (*31*) using the coordinates of one protomer of human cdN as a template. The mdN structures were solved by rigid body refinement with Refmac5.2 (*29*) using an mdN structure (pdb code 1MH9) as a template. The reflections used for R_{free} calculations on murine cdN and mdN structures were copied from the reflection files of their template structures. The refinement and model building of the murine cdN and mdN structures

Table 1: Crystallographic Data Collection and Refinement Statistics

data collection statistics	structure				
	D41N-AZTMP	D41N-BVdUMP	HcdN-dUrd	D12N-dUMP	D12N-dGMP
space group	$P4_32_12$	$P4_32_12$	$P1$	$P6_2$	$P6_2$
unit cell dimensions					
a (Å)	73.6	73.6	39.6	75.3	76.3
b (Å)	73.6	73.6	47.2	75.3	76.3
c (Å)	105.7	106.4	62.4	85.2	85.8
α (deg)	90	90	68.9	90	90
β (deg)	90	90	81.7	90	90
γ (deg)	90	90	75.0	120	120
resolution (Å)	20−1.8	40−1.95	20−1.2	65.2−1.9	66.0−2.0
$I/\sigma(I)$[a]	8.73 (3.8)	20.5 (4.8)	10.0 (3.0)	18.9 (5.5)	19.8 (4.6)
no. unique reflections	51199	27554	120312	20367	19163
redundancy of reflections	3.8	4.9	3.5	10.7	11.0
R_{sym}[a,b]	8.8 (28.8)	5.6 (35.0)	6.7 (36.5)	9.9 (35.6)	8.8 (47.8)
completeness (%)[a]	99.6 (100)	99.4 (100)	94.5 (90.8)	100 (100)	100 (100)

final refinement parameters	structure				
	D41N-AZTMP	D41N-BVdUMP	HcdN-dUrd	D12N-dUMP	D12N-dGMP
working R-value[c]	18.3	18.5	14.8	15.8	16.5
no. of reflections, working set	26052	20796	114303	19309	18178
free R-value[c]	21.4	21.6	18.1	20.4	20.5
no. of reflections, test set	1382	1122	6001	1034	985
mean B-factors (Å^2)	20.3	24.1	14.3	24.7	28.7
residues in most favorable regions (%)[d]	92.4	92.4	92.9	92.3	92.3
residues in additionally allowed regions (%)[d]	7.6	7.6	7.1	7.7	7.7
rmsd bond length (Å)	0.016	0.013	0.02	0.014	0.018
rmsd bond angles (deg)	1.471	1.426	1.7	1.422	1.560
PDB code	2JAU	2JAW	1SRW	2JAR	2JAO

[a] Numbers in parentheses are for the highest resolution shell. [b] $R_{sym} = \sum_{hkl}\sum_I |I_i(hkl) - \langle I(hkl)\rangle|/\sum_{hkl}\sum_i I_i(hkl)$ for n independent reflections and observations of a given reflection; $\langle I(hkl)\rangle$ is the average intensity of the i observations. [c] $R_{cryst} = \sum_{hkl} |F_0(hkl) - F_c(hkl)|/\sum_h |F_0(hkl)|$. [d] Ramachandran plots are made using PROCHECK Validation (*38*).

were made with Refmac5.2 (*29*) and Coot (*32*), respectively. Structural statistics are shown in Table 1.

Figures 1a, 2a, 3, 5, 8, and 9 were made with PyMol (*33*) and Figures 2b, 4, 6, and 7 with ChemDraw (Cambridge Soft Corporation).

RESULTS

Generation of Substrate and Product Complexes. To be able to study substrate recognition in cdN we had to overcome the difficulty of trapping the substrate in the active site. After the addition of substrate, the catalytic reaction immediately takes place leading to a rapid release of the nucleoside product. We used two strategies to capture substrates/products in cdN. The first was to bind a nucleoside product in the active site together with AlF_4^-, which resulted in the structure of human cdN in complex with deoxyuridine and AlF_4^- to a resolution of 1.2 Å. Fluoro-metallic compounds such as AlF_4^-, AlF_3, and BeF_3^- have previously been used to model phospho-moieties of transient reaction intermediates of HAD superfamily enzymes including phosphoserine phosphatase, mdN, cN-II, and cN-III (*14*−*16*, *34*).

The second strategy was to mutate cdN so that the substrate could remain in the active site without being hydrolyzed. Accordingly, the first Asp of Motif I (Figure 1b), which initiates the catalytic reaction by making a nucleophilic attack on the substrate, was changed to an Asn. This mutation was previously made in mdN and resulted in several structures of the inactive D41N variant of mdN in complex with substrates (*20*). For the present investigation, we first introduced this mutation in human cdN (D10N) but did not succeed in binding the substrate to the crystallized protein, presumably due to unfavorable crystal contacts. We instead made the corresponding mutation (D12N) in the 85% sequence identical murine cdN. This resulted in structures of the inactive D12N variant of murine cdN in complex with dUMP to a resolution of 1.9 Å and in complex with dGMP to a resolution of 2.0 Å.

In order to study the structural basis for nucleotide analogue recognition in the deoxyribonucleotidases, we tried to bind the nucleotide analogues AZTMP and BVdUMP in both the D12N of cdN and the D41N variant of mdN. From these attempts, we solved the structure of the D41N variant of mdN in complex with AZTMP and BVdUMP to resolutions of 1.8 and 1.9 Å, respectively.

Overall Structure of Human cdN. The structure of human cdN was solved with two polypeptides in the asymmetric unit, showing 2 × 194 (out of 201) residues that form a homodimer, which is in agreement with results from gel filtration chromatography (*6*). The structures of the two protomers differ very little from each other with an rmsd of 0.3 Å, calculated on the Cα:s using lsqcab (*35*).

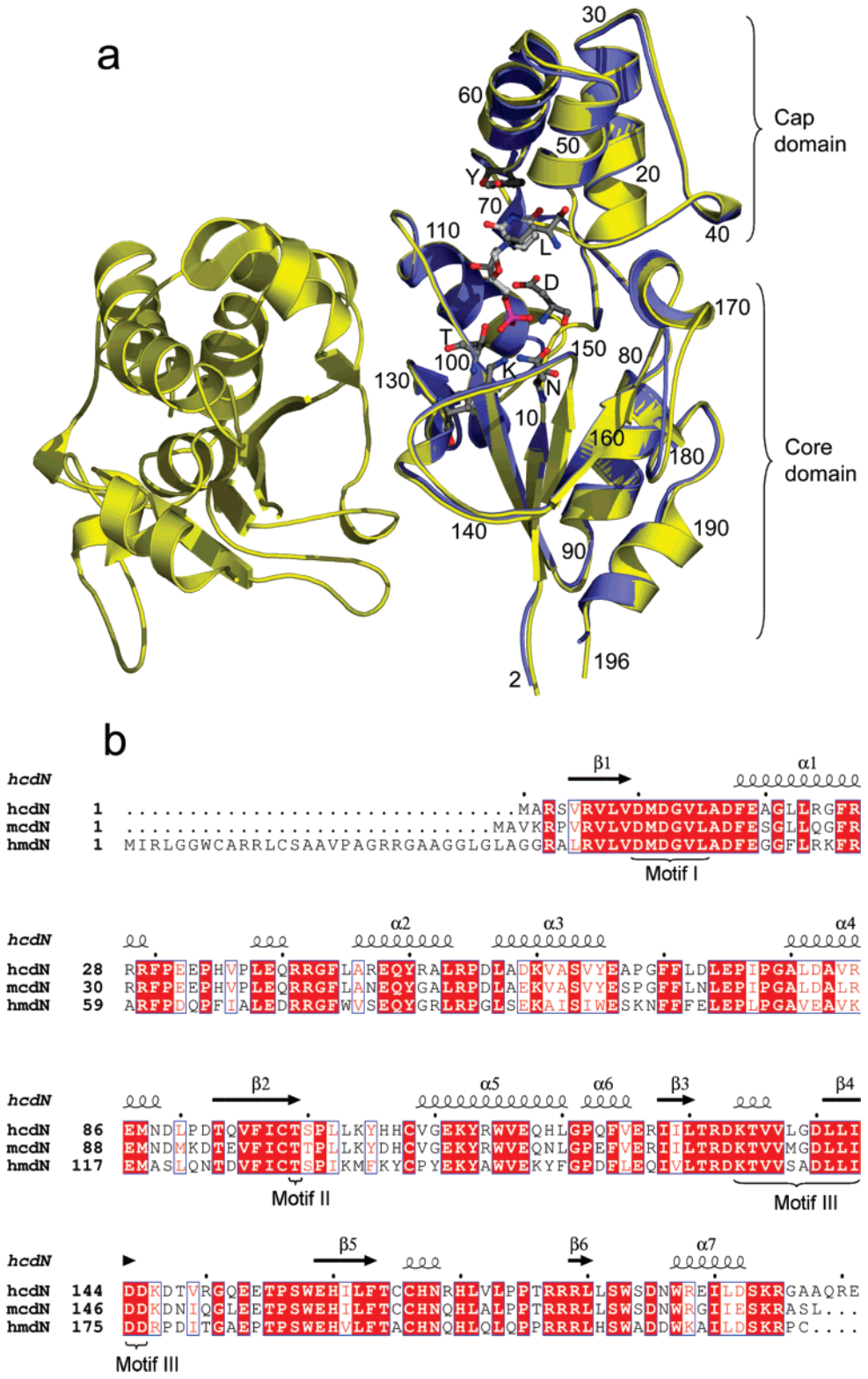

FIGURE 1: Comparisons of human and murine cdN and human mdN. (a) A superposition of the homodimeric human cdN (yellow) and one protomer of dUMP-bound D12N variant of murine cdN (blue). Numbers are residue numbers of human cdN. One-letter codes of the following residues of the D12N variant of murine cdN are shown: Asn12 and Asp14 of Motif I, Thr101 of Motif II, Lys136 of Motif III, and Leu47 and Tyr67 of the base recognition site. Nitrogens are colored in blue and oxygens in red. (b) Sequence alignment of human cdN (hcdN), murine cdN (mcdN), and human mdN (hmdN). The Swiss-Prot/TrEMBL accession numbers of the sequences used in the alignment are Q8TCD5 (human cdN), Q9JM14 (murine cdN), and Q9NPB1 (human mdN). Red fields cover completely conserved residues, and red letters in white fields represent residues that are partly conserved (have similar biochemical properties). The sequence alignment was made with ClustalW, and the image was generated with ESPript server (*39*).

cdN has two domains, an α/β Rossmann-like fold (core domain) containing six antiparallel β-strands that are sandwiched between α-helixes, and a 4-helix bundle (cap domain). In human cdN, the core domain covers residues 1−17 and 77−201, and the cap domain covers residue 18−76 (Figure 1a). It has a structure very similar to that of human

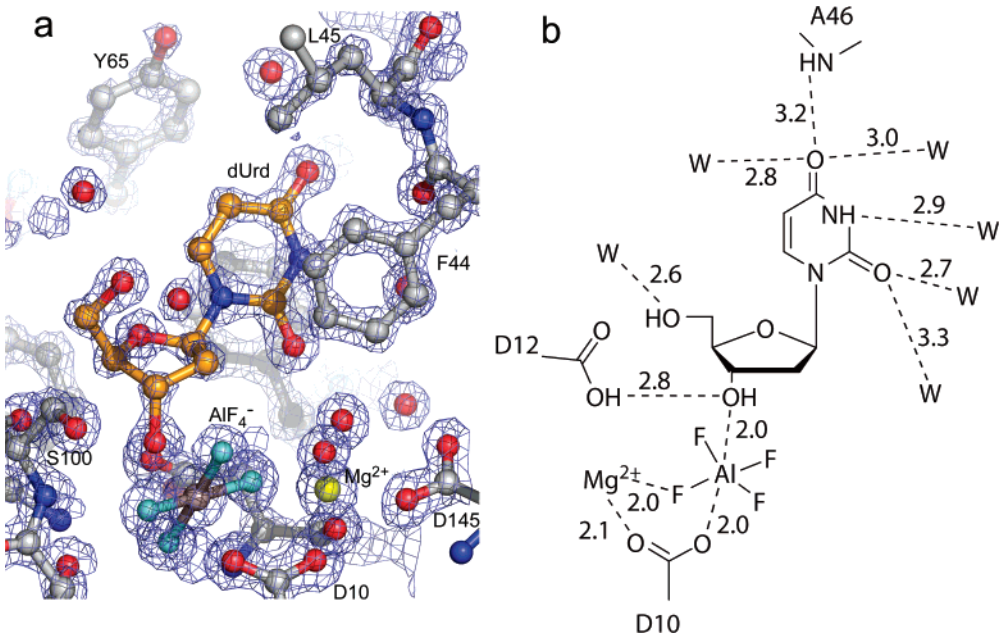

FIGURE 2: Deoxyuridine bound in the active site of human cdN. (a) A $2F_o - F_c$ electron density map contoured at 2.5σ around the active site with deoxyuridine (orange), Mg^{2+} (yellow), and AlF_4^- (light blue). (b) Schematic diagram of deoxyuridine bound in the active site showing hydrogen bond distances.

mdN with an average rmsd of 0.65 Å, comparing the Cα values of 193 residues.

The active site is situated in a cleft between the core domain and the cap domain. The core domain contains three conserved motifs that together with Mg^{2+} build up the binding site for the phosphate moiety of the substrate. Motif I (DXDX[T/V][L/V]) consists of Asp10, Asp12, Val14, and Leu15; Motif II [T/S] consists of Thr99; and Motif III $(K(X)_xD(X)_{0-4}D)$ consists of Lys134, Asp144, and Asp145 (Figure 1b). The cap domain forms an aromatic/hydrophobic pocket that coordinates the base of the nucleotide by residues Phe18, Phe44, Leu45, and Tyr65. The cap domain is less conserved than the core domain, which agrees with its role of binding the base of the nucleotide, thus determining the nucleobase specificity of the enzyme.

The residue-numbering of murine cdN and human mdN is different relative to human cdN, e.g., Asp10 in human cdN corresponds to Asp12 in murine cdN and Asp41 in human mdN (Figure 1b).

Substrate Recognition of cdN. The $F_o - F_c$ map shows well-defined density corresponding to deoxyuridine and AlF_4^- in the 1.2 Å structure of human cdN (Figure 2a). Because of this well-defined density and very high resolution, we examined the torsion angles of the two bound deoxyuridines of this dimer. The pseudorotation angles (*P*) of the two deoxyuridines were calculated, using a server (http://cactus.nci.nih.gov/prosit/) that categorizes them as having type 2′-endo ribose puckering (*36*). The AlF_4^- is closely coordinated between the 3′-hydroxyl group of deoxyuridine, and a carboxyl oxygen of Asp10 with a distance of 2.0 Å on each side (Figure 2b). By coordinating the 3′-hydroxyl group of the deoxyuridine, AlF_4^- mimics the phosphate moiety of dUMP3′. Although the Al atom is hexacoordinated, the complex resembles the hypothetic pentavalent substrate intermediate proposed in the reaction mechanism of 5′-nucleotidases (*14*). The uracil base is recognized by Ala46, Phe18, Phe44, Tyr65, and Leu45 (Figure 2). The deoxyuridine binds similarly to the thymidine moiety of dTMP3′ in mdN (*20*), suggesting that dTMP3′ and dUMP3′ are recognized in a similar way by cdN and mdN. The deoxyuridine is inverted compared to the nucleoside moiety of 5′-nucleotide substrates.

Well-defined density could be seen for both dUMP and dGMP in the D12N murine cdN from the $F_o - F_c$ OMIT electron density maps (Figure 3). Both substrates bind with the phosphate moiety in two alternative conformations (Figure 3). Similar double conformations were seen in the D41N variant of human mdN and were designated mode A and mode B (*20*). Mode A has been described as the catalytically active conformation having the 5′O atom within hydrogen bond distance to the catalytically important Asp43 of mdN (Asp14 in murine cdN), which donates a proton to the leaving nucleoside (*14*). Both dGMP and dUMP are stacked between Phe20, Phe46, Leu47, and Tyr67 of the nucleobase recognition site and form hydrogen bonds with the main chain amides of Ala48 and Asn49, the main chain carbonyl group of Thr102, and the hydroxyl group of Tyr67 and two water molecules (Figures 3 and 4). The substrate dUMP is recognized in a similar way by cdN and mdN (Figure 3b and ref *20*).

Nucleotide Analogue Recognition in Human mdN. Structures of the inactive D41N variant of human mdN were solved in complex with AZTMP and BVdUMP, which both can be dephosphorylated by mdN and cdN (*5*). Electron density corresponding to both AZTMP and BVdUMP is clearly visible in the $F_o - F_c$ OMIT electron density maps (Figure 5). The analogue BVdUMP was modeled with full occupancy with the phosphate moiety in two alternative conformations, Mode A and Mode B, similar to dUMP and dGMP in D12N (Figure 5b). The analogue AZTMP was modeled with an occupancy of 50% and binds with the phosphate moiety in Mode B.

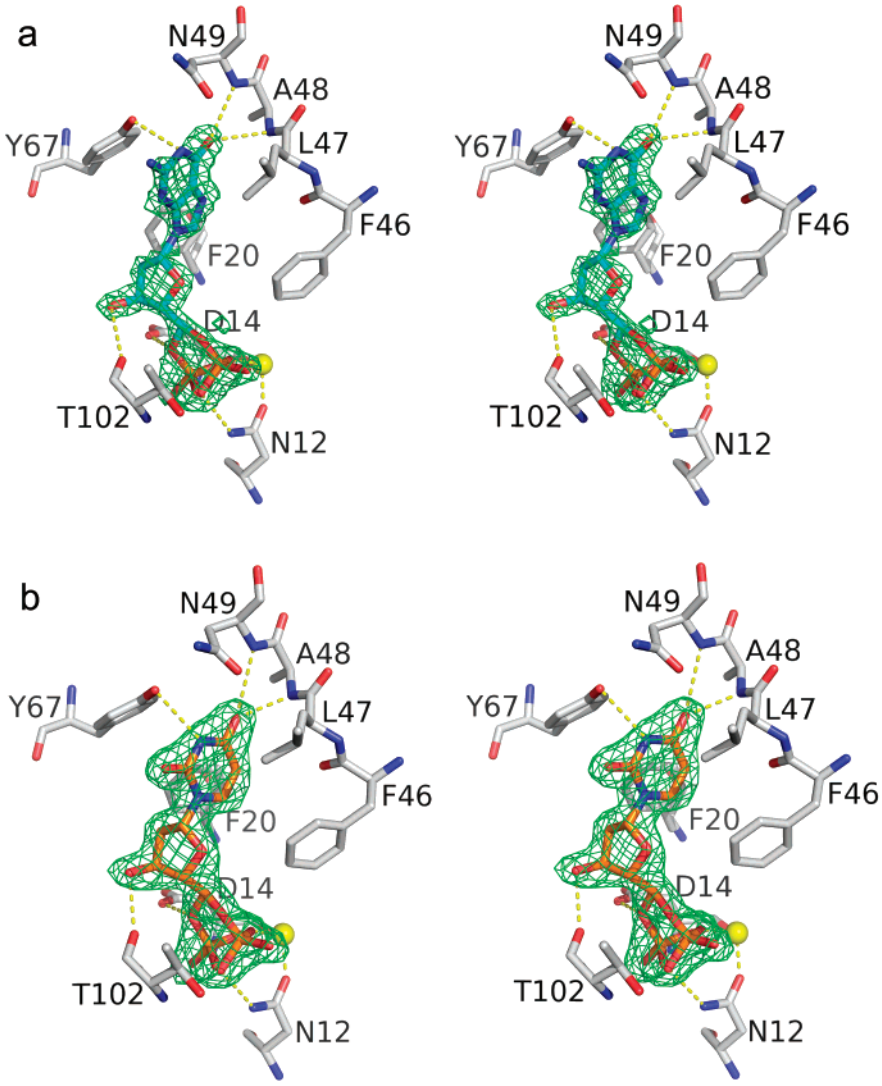

FIGURE 3: Stereo image showing $F_o - F_c$ OMIT maps covering dGMP and dUMP bound in the active site of murine cdN. (a) $F_o - F_c$ OMIT map countered at 4σ covering dGMP (turquoise). (c) $F_o - F_c$ OMIT map countered at 4σ covering dUMP (orange). Mg^{2+} is shown in yellow, nitrogens are shown in blue, and oxygens are shown in red.

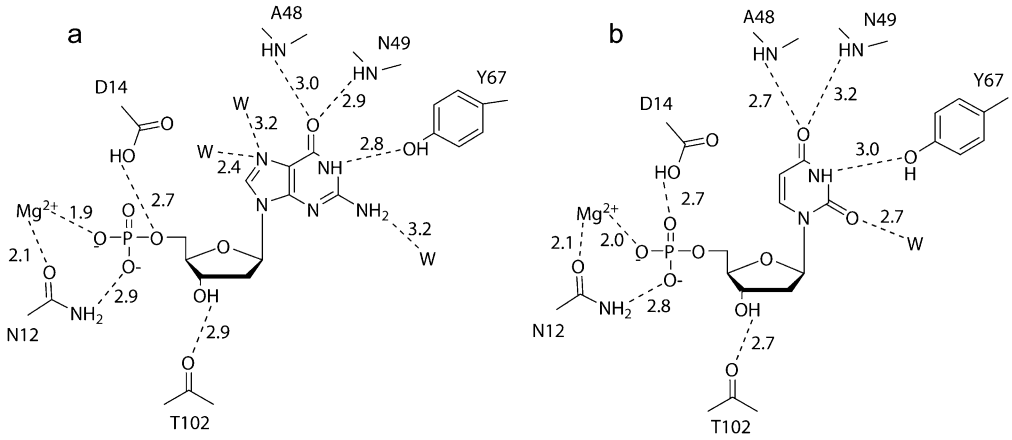

FIGURE 4: Schematic diagrams of dGMP (left) and dUMP (right) in the active site of murine cdN showing hydrogen bond distances.

The thymine base of AZTMP is stacked by Phe49, Phe75, Trp76, and Trp96 that form the nucleobase recognition site in mdN (*14*, *20*) and makes hydrogen bonds to the main chain amide groups of Val77 and Ser78 (Figures 5a and 6a). The azido group interacts with Asp43, Cys139, and the main chain amide of Ile133 and is also within short distance to the main chain carbonyl of Ser131, Phe102, and Lys143 (Figures 5a and 6a).

The bromovinyuracil base of BVdUMP is rotated 180° relative to dUMP and AZTMP, but is stacked similarly and

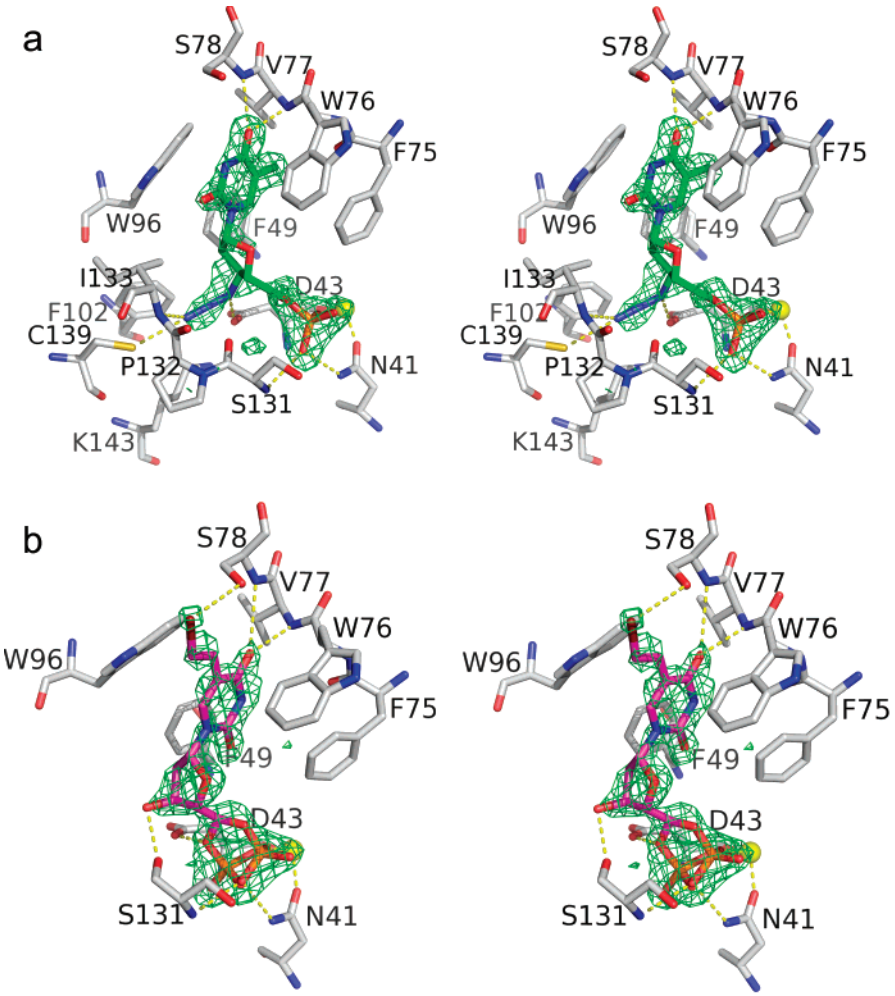

FIGURE 5: Stereo image showing $F_o - F_c$ OMIT maps of human mdN with AZTMP and BVDUMP. (a) $F_o - F_c$ OMIT map countered at 3σ covering AZTMP (green). (b) $F_o - F_c$ OMIT map countered at 4σ covering BVdUMP (purple).

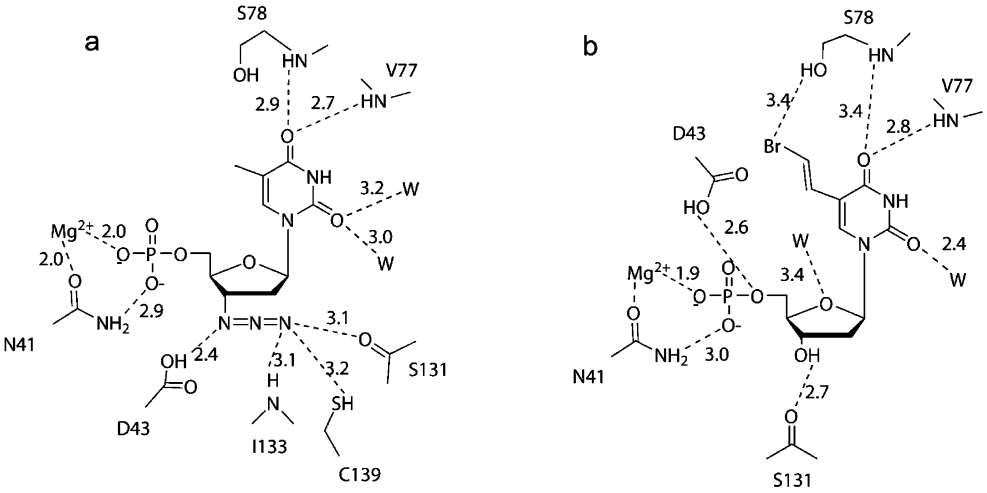

FIGURE 6: Schematic diagrams of the active site of human mdN with bound (a) AZTMP and (b) BVdUMP showing hydrogen bond distances.

forms similar hydrogen bonds (Figure 5b and ref *20*). Additionally, the bromovinyl group interacts with the side chain of Ser78 (Figures 5b and 6b).

DISCUSSION

Although the overall structures of cdN and mdN are very similar, there are differences in the nucleobase recognition sites that can account for differences in substrate specificity. Both enzymes counteract thymidine kinases in substrate cycles that regulate the size of the dNTP pools, cdN in the cytosol and mdN in the mitochondria (*37*). Mitochondrial mdN is very specific for dUMP and dTMP, whereas cdN has specificity similar to that of mdN but also accepts the purine nucleotides dGMP and dIMP. Both enzymes accept

Table 2: Substrate Specificities of Deoxyribonucleotidases

substrate	relative enzyme activity, %		
	human cdN[a]	murine cdN[b]	human mdN[c]
dUMP	100	100	100
dTMP	55	65	50
dCMP	0.7	16	0
dAMP	13	9	2
dGMP	81	45	6
dTMP3′	ND[d]	58	77
UMP3′	76	35	47

[a] The relative enzyme activities are taken from ref *6*, which also reports K_m and V_{max} values for the individual enzymes. [b] The relative enzyme activities are taken from ref *7*, which also reports K_m and V_{max} values for the individual enzymes. [c] The relative enzyme activities are taken from ref *4*, which also reports K_m and V_{max} values for the individual enzymes. [d] ND: not determined.

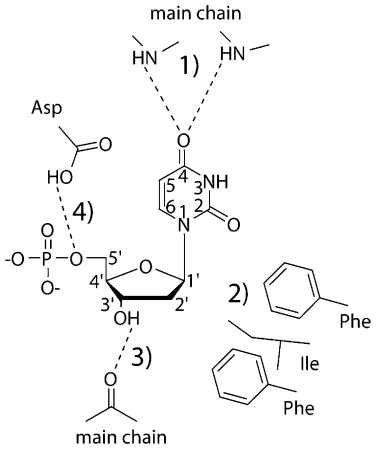

FIGURE 7: Schematic diagram showing two recognition sites (1 and 2) shared by cdN and mdN that provide the specificity toward the deoxyribo form of 4-hydoxypyrimidine nucleotides. Furthermore, it points out interactions (3 and 4) that are crucial for efficient catalysis.

uracil- and thymine-based 2′,3′-nucleotides as substrates. Relative activities are listed in Table 2.

The deoxyribonucleotidases cdN and mdN have almost identical catalytic phosphate binding sites that contain the conserved motifs found in most HAD superfamily enzymes. In recognizing the nucleobase moiety of the substrate, they also share a specific recognition site for the 4-carbonyl group of the pyrimidine base (Figure 7) (*20*). The site contains two main chain amides that form favorable hydrogen bonds with the 4-carbonyl group of dUMP and dTMP, but it would repel the 4-amino group of dCMP. In cdN, this is also a binding site for the 6-carbonyl group of dGMP and dIMP and makes the enzyme reject dAMP as substrate. Furthermore they both contain the hydrophobic/aromatic residues Ile and Phe close to the 2′C of the ribose, efficiently making cdN and mdN favor the deoxyribo form over the ribo form of 5′-nucleotides (Figure 7) (*20*).

We can correlate the differences in the nucleobase recognition site between cdN and mdN with their different capacities to dephosphorylate purine nucleotides, by superposing the cdN-dGMP structure with the previously solved mdN-dGMP structure (Figure 8). From this, we conclude that residues Leu47 and Tyr67 of cdN form a more favorable surface for interaction with dGMP than the corresponding Trp76 and Trp96 in mdN (Figure 8). Probably residues Trp76 and Trp96 in mdN are responsible for the preference of mdN for pyrimidine over purine nucleotides (Table 2).

During catalysis, formation of a hydrogen bond between O5′ and Asp43 (Asp14 in murine cdN) is probably required, since this Asp is proposed to donate a proton to generate the 5′-hydroxyl group of the leaving nucleoside product (*14*). Figure 8 shows that dGMP binds in mdN with the phosphate moiety slightly displaced from the phosphate binding site, so that the O5′ is not within hydrogen bond distance to Asp43. This correlates with dGMP being hydrolyzed less efficiently in mdN (*20*).

Studies have shown that deoxyribonucleotidases can dephosphorylate and therefore deactivate several nucleoside analogues (Table 3) (*5*). In order to study how the deoxyribonucleotidases recognize nucleoside analogues commonly used for antiviral therapy we solved the structure of mdN in complex with AZTMP and BVdUMP.

In mdN, AZTMP binds in the same orientation as dTMP, with the thymine and phosphate moieties in almost identical locations (Figure 9a) but with the sugar moiety with its bulky 3′-azido group (N═N═N−) in a strained conformation. The 3′- and 4′C of the sugar are bent upward relative to dTMP, and the 5′C is in a different position (Figure 9a) most likely because the azido group forces the ribose into this conformation, being too large to fit in the binding pocket of the 3′-hydroxyl group. The bad fit of the azido group probably causes a large decrease in binding affinity relative dTMP,

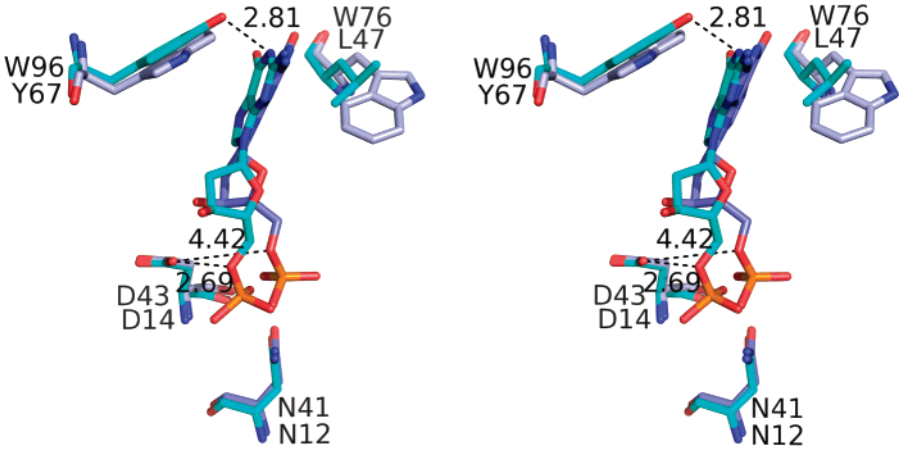

FIGURE 8: Stereo image of the active site of murine cdN with bound dGMP (turquoise) superposed on the previously solved mdN-dGMP structure (light blue) (*20*).

Table 3: Comparison of Substrate Activities for AZTMP and BVdUMP with Those for the Physiological Substrates dUMP and dTMP[a]

	human mdN			human cdN			murine cdN		
substrate	K_m (mM)	V_{max} (units/mg)	V_{max}/K_m	K_m (mM)	V_{max} (units/mg)	V_{max}/K_m	K_m (mM)	V_{max} (units/mg)	V_{max}/K_m
dUMP	0.1	110	1100	1.5	49	33	0.8	110	138
dTMP	0.2	74	370	1.5	64	43	1.4	156	111
AZTMP	2.5	8.4	3.4	2.4	21	9	3.6	238	66
BVdUMP	0.7	56	80	1.9	6	3	2.8	38	14

[a] All values are taken from a previous publication (*5*) and were measured at pH 7.5. One unit of enzyme activity corresponds to the dephosphorylation of 1 μmol substrate per min.

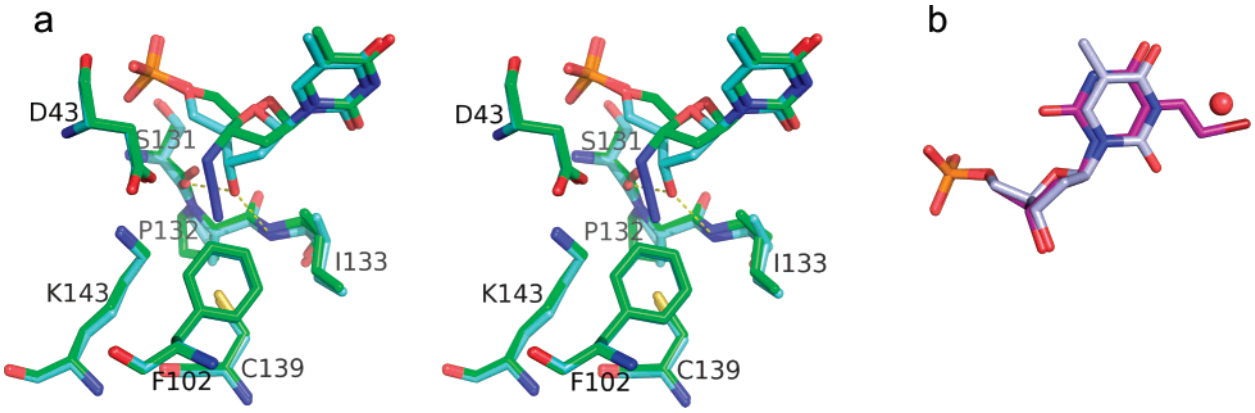

FIGURE 9: Nucleotide analogue recognition in mdN. (a) Stereo image of the active site of mdN with bound AZTMP (green) superposed on the mdN-dTMP structure (light blue) (*20*). (b) The mdN-bound BVdUMP (purple) superposed on the mdN-bound dTMP (light blue) (*20*).

which is reflected in the K_m values (Table 3). AZTMP binds with the phosphate moiety in Mode B. However, the 5′C is positioned so that the phosphate cannot reach the catalytically active Mode A just by rotating around the 5′C as observed with dUMP and dGMP in cdN. Similarly to the mdN-bound dGMP, the 5′O is not within hydrogen bond distance to Asp43 (Figure 9a), which lowers the rate of delivery of the carboxyl proton. The close interaction of the azido group with Asp43 (Figure 9a) might also affect the catalytic efficiency.

The 3′-hydroxyl group of the 5′-substrates interacts closely with the main chain in both cdN (Figures 4−7) and mdN (*20*), an interaction probably required for high activity (Figure 7 and ref *20*). This together with the poor fit of the 3′-azido group of AZTMP (Figure 5a) suggests that a substitution at the 3′-position of the ribose might be an efficient way to decrease the affinity of deoxyribonucleotidases toward nucleoside analogues.

In mdN, the bromovinyuracil base of BVdUMP is inverted relative to the thymine base (Figure 9b). The bromovinyl group replaces a water molecule and makes a hydrogen bond to the side chain of Ser78 (Figures 9b and 6). The sugar and phosphate moieties of BVdUMP bind almost identically as in dTMP, which implies that the catalytic efficiency should be only marginally affected since the interactions with the catalytically important residues are not changed. This correlates with it being a relatively good substrate for mdN compared to AZTMP and other nucleoside analogues (Table 3 and ref *5*).

In conclusion, the present study adds further insights into the detailed structural basis for the substrate specificity of human 5′-nucleotidases and is another step in our efforts to provide a complete structural description of all human 5′-nucleotidases. A complete description of the specificity determinants of these enzymes, together with similar studies of the human nucleotide kinases, is likely to be of significant value for future efforts at developing catabolically stable nucleotide-based drugs as well as to provide a structural basis for drug resistance mutations seen in these enzymes. The studies will also provide a comprehensive view for how an evolutionary family has been modulated to provide useful substrate specificity distributions of each enzyme, which together allow appropriate nucleotide pools to be maintained for different cellular requirements.

ACKNOWLEDGMENT

We thank the staff on X11 at EMBL Hamburg Outstation, on I711 and I911 at Max Lab, and on ID14.4 at European Synchrotron Radiation Facility for technical assistance. We are also grateful to Karl-Magnus Larsson and Pål Stenmark for help with data collection of the human cdN data.

REFERENCES

1. Reichard, P. (1988) Interactions between Deoxyribonucleotide and DNA-Synthesis, *Annu. Rev. Biochem. 57*, 349−374.
2. Bianchi, V., and Spychala, J. (2003) Mammalian 5′-nucleotidases, *J. Biol. Chem. 278*, 46195−46198.
3. Hunsucker, S. A., Mitchell, B. S., and Spychala, J. (2005) The 5′-nucleotidases as regulators of nucleotide and drug metabolism, *Pharmacol. Ther. 107*, 1−30.
4. Rampazzo, C., Gallinaro, L., Milanesi, E., Frigimelica, E., Reichard, P., and Bianchi, V. (2000) A deoxyribonucleotidase in mitochondria: involvement in regulation of dNTP pools and possible link to genetic disease, *Proc. Natl. Acad. Sci., U.S.A. 97*, 8239−8244.
5. Mazzon, C., Rampazzo, C., Scaini, M. C., Gallinaro, L., Karlsson, A., Meier, C., Balzarini, J., Reichard, P., and Bianchi, V. (2003) Cytosolic and mitochondrial deoxyribonucleotidases: activity with

substrate analogs, inhibitors and implications for therapy, *Biochem. Pharmacol. 66*, 471−479.
6. Höglund, L., and Reichard, P. (1990) Cytoplasmic 5′(3′)-Nucleotidase from Human Placenta, *J. Biol. Chem. 265*, 6589−6595.
7. Rampazzo, C., Johansson, M., Gallinaro, L., Ferraro, P., Hellman, U., Karlsson, A., Reichard, P., and Bianchi, V. (2000) Mammalian 5′(3′)-deoxyribonucleotidase, cDNA cloning, and overexpression of the enzyme in Escherichia coli and mammalian cells, *J. Biol. Chem. 275*, 5409−5415.
8. Carson, D. A., Carrera, C. J., Wasson, D. B., and Iizasa, T. (1991) Deoxyadenosine-resistant human T lymphoblasts with elevated 5′- nucleotidase activity, *Biochim. Biophys. Acta 1091*, 22−28.
9. Hunsucker, S. A., Spychala, J., and Mitchell, B. S. (2001) Human cytosolic 5′-nucleotidase I - Characterization and role in nucleoside analog resistance, *J. Biol. Chem. 276*, 10498−10504.
10. Lotfi, K., Mansson, E., Chandra, J., Wang, Y. Y., Xu, D. W., Knaust, E., Spasokoukotskaja, T., Liliemark, E., Eriksson, S., and Albertioni, F. (2001) Pharmacological basis for cladribine resistance in a human acute T lymphoblastic leukaemia cell line selected for resistance to etoposide, *Br. J. Haematol. 113*, 339−346.
11. Schirmer, M., Stegmann, A. P. A., Geisen, F., and Konwalinka, G. (1998) Lack of cross-resistance with gemcitabine and cytarabine in cladribine-resistant HL60 cells with elevated 5′-nucleotidase activity, *Exp. Hematol. 26*, 1223−1228.
12. Galmarini, C. M., Thomas, X., Graham, K., El, Jafaari, A., Cros, E., Jordheim, L., Mackey, J. R., and Dumontet, C. (2003) Deoxycytidine kinase and cN-II nucleotidase expression in blast cells predict survival in acute myeloid leukaemia patients treated with cytarabine, *Br. J. Haematol. 122*, 53−60.
13. Kawasaki, H., Carrera, C. J., Piro, L. D., Saven, A., Kipps, T. J., and Carson, D. A. (1993) Relationship of Deoxycytidine Kinase and Cytoplasmic 5′-Nucleotidase to the Chemotherapeutic Efficacy of 2-Chlorodeoxyadenosine, *Blood 81*, 597−601.
14. Rinaldo-Matthis, A., Rampazzo, C., Reichard, P., Bianchi, V., and Nordlund, P. (2002) Crystal structure of a human mitochondrial deoxyribonucleotidase, *Nat. Struct. Biol. 9*, 779−787.
15. Walldén, K., Stenmark, P., Nyman, T., Flodin, S., Gräslund, S., Loppnau, P., Bianchi, V., and Nordlund, P. (2007) Crystal structure of human cytosolic 5′-nucleotidase II: Insights into allosteric regulation and substrate recognition, *J. Biol. Chem. 282*, 17828−17836.
16. Bitto, E., Bingman, C. A., Wesenberg, G. E., McCoy, J. G., and Phillips, G. N. (2006) Structure of pyrimidine 5′-nucleotidase type 1 - Insight into mechanism of action and inhibition during lead poisoning, *J. Biol. Chem. 281*, 20521−20529.
17. Lahiri, S. D., Zhang, G. F., Dunaway-Mariano, D., and Allen, K. N. (2003) The pentacovalent phosphorus intermediate of a phosphoryl transfer reaction, *Science 299*, 2067−2071.
18. Allegrini, S., Pesi, R., Tozzi, M. G., Fiol, C. J., Johnson, R. B., and Eriksson, S. (1997) Bovine cytosolic IMP/GMP-specific 5′-nucleotidase: cloning and expression of active enzyme in Escherichia coli, *Biochem. J. 328*, 483−487.
19. Collet, J. F., Stroobant, V., Pirard, M., Delpierre, G., and Van Shaftingen, E. (1998) A new class of phosphotransferases phosphorylated on an aspartate residue in an amino-terminal DXDX-(T/V) motif, *J. Biol. Chem. 273*, 14107−14112.
20. Wallden, K., Ruzzenente, B., Rinaldo-Matthis, A., Bianchi, V., and Nordlund, P. (2005) Structural basis for substrate specificity of the human mitochondrial deoxyribonucleotidase, *Structure 13*, 1081−1088.
21. Furman, P. A., Fyfe, J. A., Stclair, M. H., Weinhold, K., Rideout, J. L., Freeman, G. A., Lehrman, S. N., Bolognesi, D. P., Broder, S., Mitsuya, H., and Barry, D. W. (1986) Phosphorylation of 3′-Azido-3′-deoxythymidine and Selective Interaction of the 5′-Triphosphate with Human-Immunodeficiency-Virus Reverse-Transcriptase, *Proc. Natl. Acad. Sci. U.S.A. 83*, 8333−8337.
22. Lewis, W., Day, B. J., and Copeland, W. C. (2003) Mitochondrial toxicity of NRTI antiviral drugs: An integrated cellular perspective, *Nat. Rev. Drug Discovery 2*, 812−822.
23. De, Clercq, E. (2005) (E)5-(2-bromovinyl)-2′ deoxyuridine (BVDU), *Med. Res. Rev. 25*, 1−20.
24. Bradford, M. M. (1976) Rapid and Sensitive Method for Quantitation of Microgram Quantities of Protein Utilizing Principle of Protein-Dye Binding, *Anal. Biochem. 72*, 248−254.
25. Kabsch, W. (1988) Automatic-Indexing of Rotation Diffraction Patterns, *J. Appl. Crystallogr. 21*, 67−71.
26. Leslie, A. G. W. (1992) Recent changes to the MOSFLM package for processing film and image plate data, *Joint CCP4 + ESF-EAMCB Newsletter on Protein Crystallography 26*.
27. Kabsch, W. (1988) Evaluation of Single-Crystal X-Ray-Diffraction Data from a Position-Sensitive Detector, *J. Appl. Crystallogr. 21*, 916−924.
28. Brunger, A. T., Adams, P. D., Clore, G. M., DeLano, W. L., Gros, P., Grosse-Kunstleve, R. W., Jiang, J. S., Kuszewski, J., Nilges, M., Pannu, N. S., Read, R. J., Rice, L. M., Simonson, T., and Warren, G. L. (1998) Crystallography & NMR system: A new software suite for macromolecular structure determination, *Acta Crystallogr. D 54*, 905−921.
29. Murshudov, G. N., Vagin, A. A., and Dodson, E. J. (1997) Refinement of macromolecular structures by the maximum-likelihood method, *Acta Crystallogr. D 53*, 240−255.
30. Harding, M. M. (2006) Small revisions to predicted distances around metal sites in proteins, *Acta Crystallogr. D 62*, 678−682.
31. Vagin, A., and Teplyakov, A. (1997) MOLREP: an automated program for molecular replacement, *J. Appl. Crystallogr. 30*, 1022−1025.
32. Emsley, P., and Cowtan, K. (2004) Coot: model-building tools for molecular graphics, *Acta Crystallogr. D 60*, 2126−2132.
33. DeLano, W. L. (2002) *The PyMOL Molecular Graphics System*, DeLano Scientific, Palo Alto, CA, U.S.A.
34. Wang, W. R., Cho, H. S., Kim, R., Jancarik, J., Yokota, H., Nguyen, H. H., Grigoriev, I. V., Wemmer, D. E., and Kim, S. H. (2002) Structural characterization of the reaction pathway in phosphoserine phosphatase: Crystallographic "snapshots" of intermediate states, *J. Mol. Biol. 319*, 421−431.
35. Kabsch, W. (1976) Solution for Best Rotation to Relate 2 Sets of Vectors, *Acta Crystallogr. A 32*, 922−923.
36. Bloomfield, V. A., Crothers, D. M., and Tinoco, I., Jr. (2000) *Nucleic Acids: Structures, Properties and Functions*, University Science Books, Sausalito, CA.
37. Rampazzo, C., Ferraro, P., Pontarin, G., Fabris, S., Reichard, P., and Bianchi, V. (2004) Mitochondrial deoxyribonucleotides, pool sizes, synthesis, and regulation, *J. Biol. Chem. 279*, 17019−17026.
38. Laskowski, R. A., Macarthur, M. W., Moss, D. S., and Thornton, J. M. (1993) Procheck - a Program to Check the Stereochemical Quality of Protein Structures, *J. Appl. Crystallogr. 26*, 283−291.
39. Gouet, P., Courcelle, E., Stuart, D. I., and Metoz, F. (1999) ESPript: analysis of multiple sequence alignments in PostScript, *Bioinformatics 15*, 305−308.

BI7014794